

# Validation of Kalman Filter alignment algorithm with cosmic-ray data using a CMS silicon strip tracker endcap

D. Sprenger, M. Weber<sup>1)</sup>, R. Adolphi, R. Brauer, L. Feld, K. Klein, A. Ostapchuk, S. Schael, B. Wittmer

*RWTH Aachen University, I. Physikalisches Institut, Aachen, Germany*

## Abstract

A Kalman Filter alignment algorithm has been applied to cosmic-ray data. We discuss the alignment algorithm and an experiment-independent implementation including outlier rejection and treatment of weakly determined parameters. Using this implementation, the algorithm has been applied to data recorded with one CMS silicon tracker endcap. Results are compared to both photogrammetry measurements and data obtained from a dedicated hardware alignment system, and good agreement is observed.

---

<sup>1)</sup> Now at University of Hamburg, Hamburg, Germany

# 1 Introduction

Today's tracking detectors in particle physics experiments consist of several hundreds up to ten thousands of independent detector elements, which allow to measure charged particle trajectories with a single-point resolution of typically 10–50  $\mu\text{m}$  [1, 2, 3]. This resolution is significantly better than the placement accuracy as achieved during construction, which typically is an order of magnitude larger. The established method to determine the true detector element position and orientation is to use measurements from particles traversing the detector in-situ, minimizing the residuals of an appropriate track model. Several algorithms have been proposed and exposed to data [4, 5]. In this note we discuss the implementation and application of an alignment algorithm based on the Kalman Filter [6] to tracks from cosmic muons recorded by an integration setup of one CMS Tracker Endcap [7], detailing the algorithm and summarizing results from reference [8]. The algorithmic implementation is done in a portable, experiment-independent manner and easily allows application in other experiments as well.

## 2 Kalman Filter alignment algorithm

The Kalman Filter algorithm has been implemented mainly according to the formulæ described in reference [6] with some modifications.

The vector  $\vec{m}$  of detector measurements on a particle track is described by a function  $\vec{f}$  that depends both on the track parameters  $\vec{p}$  and the alignment parameters  $\vec{a}$ ,

$$\vec{m} = \vec{f}(\vec{p}, \vec{a}) + \vec{\epsilon}, \quad (1)$$

where the measurement errors are described by  $\vec{\epsilon}$ , which has a known covariance matrix  $C$ . If the function  $\vec{f}$  is not linear in the parameters  $(\vec{p}, \vec{a})$ , it is linearized at a starting point  $(\vec{p}_0, \vec{a}_0)$ :

$$\vec{m} = \vec{f}(\vec{p}_0, \vec{a}_0) + H(\vec{p} - \vec{p}_0) + D(\vec{a} - \vec{a}_0) + \vec{\epsilon} + \mathcal{O}((\vec{p} - \vec{p}_0)^2, (\vec{a} - \vec{a}_0)^2) \quad (2)$$

$$\approx \underbrace{\vec{f}(\vec{p}_0, \vec{a}_0) - H\vec{p}_0 - D\vec{a}_0}_{\vec{\epsilon}} + H\vec{p} + D\vec{a} \quad (3)$$

where the Jacobians  $H$  and  $D$  are

$$H = \frac{\partial \vec{f}}{\partial \vec{p}}(\vec{p}_0, \vec{a}_0), \quad D = \frac{\partial \vec{f}}{\partial \vec{a}}(\vec{p}_0, \vec{a}_0). \quad (4)$$

Typically, for the expansion point  $\vec{a}_0$  the design geometry, knowledge from the assembly, or a previous alignment is chosen, and  $\vec{p}_0$  are the track parameters obtained with this geometry.

The goal of the Kalman Filter algorithm is to minimize the track residuals, i. e. to minimize the objective function

$$f_{obj} = (\vec{m} - \vec{f}(\vec{p}, \vec{a}))^T C (\vec{m} - \vec{f}(\vec{p}, \vec{a})) \quad (5)$$

for the given track sample. This is achieved processing tracks in sequence and updating parameters and covariance matrix after each track. The resulting update equations for the alignment parameters  $\vec{a}$  and their covariance matrix  $E$  are [6, 9]

$$\hat{\vec{a}} = \vec{a} + ED^T W (\vec{m} - \vec{\epsilon} - D\vec{a}) \quad (6)$$

$$\hat{E} = E - (ED^T)^T \cdot W \cdot ED^T \quad (7)$$

Here,  $W$  and  $V$  are auxiliary matrices, given by [9]

$$W = V^{-1} - V^{-1}H(H^T V^{-1}H)^{-1}H^T V^{-1}, \quad V = C + DED^T. \quad (8)$$

Alignment parameters  $\vec{a}$  and covariance matrix  $E$  are updated with each track. The algorithm needs a starting point for the parameters  $\vec{a}$  and their covariance matrix  $E$ , which can be set to expectations e. g. from assembly tolerances. If in doubt, larger initial uncertainties are preferred since too small values can bias the alignment because the covariance matrix has decreasing eigenvalues. Parameters corresponding to global degrees of freedom can be fixed by assigning tiny prior uncertainties to specific alignment parameters.

In order to avoid bias from mis-measured tracks in the first steps, deterministic annealing with a configurable geometric schedule can be applied. This is done by increasing measurement uncertainties in Equation (8):

$$V = \alpha(k)C + DED^T, \quad \alpha(k) = \begin{cases} b^{\frac{n-k}{n-1}} & \text{for } 1 \leq k \leq n, \\ 1 & \text{for } k > n \end{cases} \quad (9)$$

Here,  $k$  denotes the number of the current track,  $b$  is the annealing factor which is applied to the covariance matrix in the first step, and  $n$  is the number of the track from which on the full information from the track is kept.

### 3 Implementation

The software implementation of the algorithm has been done in an experiment-independent way. However, the input data are obtained from a specialized software framework tailored to the experiment, usually providing pattern recognition, track reconstruction as well as the description of the geometrical layout of the detector elements. Therefore, an interface between the experiment specific and the experiment independent software was designed. The basic choice was made that the experiment specific implementation has to provide all the information that is necessary to compute Equations (6)–(8) in a persistent matrix format, plus some additional information.

#### 3.1 Experiment specific implementation

In the experiment specific implementation, the first additional information to be provided and stored is the number of parameters to be aligned. Parameters need to be identified uniquely by an index. This is necessary to save space and speed up the computation. The reason is that the Jacobian  $D$  in Eq. (4) has only few entries different from zero, since a single track only crosses few detector elements.

A rough selection of tracks suitable for alignment has to be done, judging on the current alignment parameters. Then, for each track, the experiment specific software has to supply the measurement  $\vec{m}$  with its covariance  $C$ , the constant  $\vec{c}$ , and the Jacobians  $H$  and  $D$ . The Jacobians are evaluated according to the current knowledge at non-optimal parameters  $\vec{p}_0$  and  $\vec{a}_0$ <sup>1)</sup>.

Additional experiment dependent information can be supplied, like run and event numbers and the number of the track in the current event. This can be especially useful if some tracks are rejected as outliers in the alignment procedure, such that one can have a look at the corresponding events within the experiment dependent software (e. g. event display). Also the value  $\tilde{\chi}^2$  of the track fit, defined as

$$\tilde{\chi}^2 = \vec{r}^T C \vec{r} \quad \text{with} \quad \vec{r} = (\vec{m} - \vec{c}) \quad (10)$$

and the number of degrees of freedom  $n_{dof}$  in the fit are stored. One has to note that in the case of an unaligned detector,  $\tilde{\chi}^2$  does not follow a  $\chi^2$ -distribution, but still provides some power to discriminate bad tracks.

#### 3.2 Implementation of the Kalman Filter alignment algorithm

The Kalman Filter alignment algorithm is implemented as a C++ program, which uses the ROOT [10] data analysis framework. The program reads the needed track information from the files which were created with the experiment specific program.

The program initializes a vector of alignment parameters and the corresponding covariance matrix with configurable starting values. One option is to pass over this information from the experiment specific part. However, pattern recognition and track reconstruction are very costly time-wise, and input values to alignment only change little (e. g. due to non-linearities of  $\vec{f}(\vec{p}, \vec{a})$ , which are neglected in Equation (3)) when a different starting point is taken. By choosing the initialization to happen in the experiment independent part, avoiding a new reconstruction, computing time is saved.

Then, processing track after track, the parameters  $\vec{a}$  and the covariance matrix  $E$  are updated as specified in Equations (6) and (7). Memory and computing time are saved in this step by reducing the alignment derivatives matrix  $D$  to non-zero columns, which correspond to the detector elements hit by the current track. In the same spirit, computing time is saved by using only the (known) non-zero elements of  $D^T$  when computing the product

<sup>1)</sup> A reference implementation in C++ [11] for the CMS experiment is available and can be used as a template for other experiments.

$ED^T$ . The matrix  $ED^T$  consists of one line for each alignment parameter (not only those hit by the current track), and one column for each single measurement of the current track. The most computing time intensive matrix operation is the update of the matrix  $E$ , which is quadratic in the number of parameters and dominates the time consumption of the alignment procedure in case of many alignment parameters.

During the update, the current alignment parameters and their uncertainties (extracted from the diagonal elements of the covariance matrix) are filled into histograms. After all tracks have been processed, these histograms together with the final parameters, their uncertainties, and additional information on the alignment procedure like the number of hits for each detector element are stored.

### 3.2.1 Outlier rejection

To prevent bad measurements (e. g. from noise clusters) from having a large impact on the alignment results, outlier rejection is implemented. As mentioned above, the value  $\tilde{\chi}^2$  (cf. Eq. (10)) is computed for each track. The track is used for updating  $\vec{a}$  and  $E$  when the probability  $P(\tilde{\chi}^2, n_{dof})$  exceeds a configurable threshold value.

An additional outlier rejection is implemented by rejecting tracks that change the alignment parameters by more than a configurable factor beyond their uncertainties. Tracks showing this effect are assumed to be wrongly measured. Considering the fact that the current alignment parameters combine the information of all previously processed tracks, one additional track should not have such a large impact on the results.

### 3.2.2 Weakly determined parameters

The objective function (5) is invariant under a global translation and rotation of all detector elements, i. e. a special linear transformation of the alignment parameters. Even when not present in the starting values  $\vec{a}$  and  $E$ , such transformations can build up due to mis-measurements, round-off problems in the alignment procedure, or an incomplete track model. Large alignment parameters  $\vec{a}$  have a negative impact on the alignment procedure due to larger distance to the linearization point. Therefore, these global parameters should be fixed. This can be achieved by assigning small uncertainties to some (linear combinations of) parameters for the initial matrix  $E$ , depending on the experimental setup, which corresponds to the definition of a geometry reference system.

Furthermore, large eigenvalues can be present in  $E$  even after processing the last track. These large eigenvalues correspond to certain linear combinations of alignment parameters which geometrically represent a systematic distortion of the detector units position and orientation that is only weakly determined. This happens especially if the track sample consists of tracks with similar topology. Artificial distortions can bias physics observables like invariant masses, momentum scale etc.

We consider two methods to suppress weak modes: The first method is to assign a small initial error to the weakly determined linear combination of parameters in  $E$ . The alternative is to align without changing the initial values of  $E$ , and later fit the amplitude of the weakly determined mode and subtract it from the parameters.

## 4 Application to data

The Kalman Filter alignment algorithm was applied to data taken from the integration setup of one endcap of the CMS experiment [3, 7] tracker (TEC+). The integration took place in 2006 at RWTH Aachen University. Apart from commissioning the system hardware, tracks from cosmic muons originating from air-showers were recorded and used for alignment.

### 4.1 CMS Tracker Endcap

The CMS tracker [3] is entirely based on silicon detector technology. It can be divided into five subsystems (Fig. 1): Pixel detector (PIXEL), Tracker Inner Barrel (TIB), Tracker Outer Barrel (TOB), Tracker Inner Disks (TID+, TID-), and Tracker Endcaps (TEC+, TEC-).

CMS uses the following coordinate definitions: The  $y$ -axis points upwards, the  $x$ -axis points radially to the centre of the LHC [12] ring, and the  $z$ -axis points in direction of the beam line, completing a right-handed coordinate system. The azimuthal angle  $\phi$  is measured to the  $x$ -axis in the  $x$ - $y$ -plane, and hence describes rotations around the  $z$ -axis, and the polar angle  $\theta$  is measured to the  $z$ -axis.

The Tracker Endcap TEC+ covers the range  $0.9 \leq \eta \leq 2.5$  and consists of 3200 trapezoidal silicon-strip detectors. Both TECs consist of nine disks (Fig. 2) carrying 16 substructures called petals. Eight petals are mounted on the

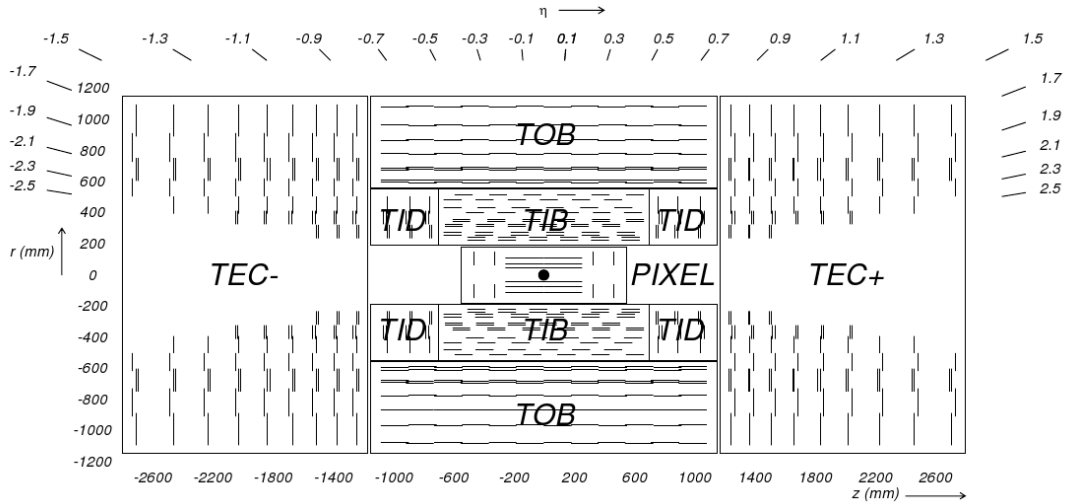


Figure 1: View of the CMS tracker in the  $rz$ -plane [3]. Each line in the strip tracker represents a silicon strip detector, whereas lines in the pixel detector represent ladders and petals on which the detectors are mounted in the barrel and endcaps, respectively.

side facing the interaction point (front petals) and eight on the far side (back petals). By grouping the neighbouring front and back petals, the disks are divided into eight sectors numbered from 1 to 8. On the petals (Fig. 3), detectors are mounted with the strips in radial direction in up to seven rings.

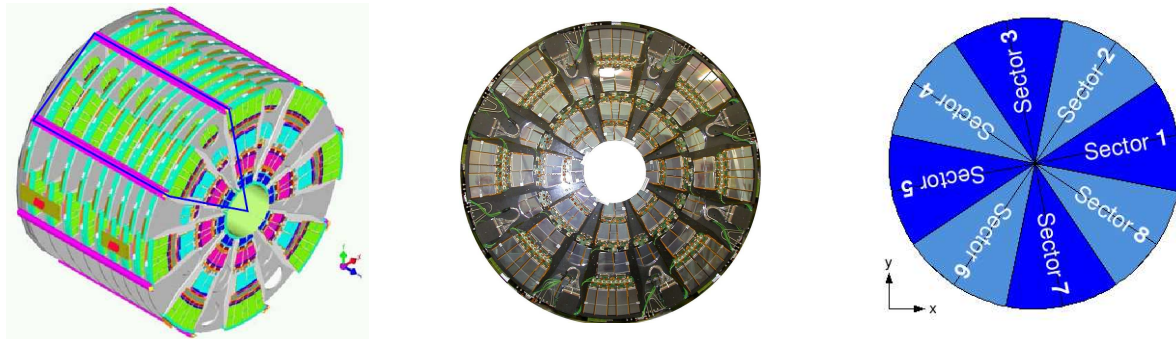


Figure 2: Left: Sketch of a tracker endcap [3]. Middle: Photo of a TEC disk. Right: Sector numbering scheme.

## 4.2 Sector tests

Petals in TEC+ were integrated and commissioned sector by sector. The petals were mounted and subsequently attached to services (cooling, power, trigger, communication and data lines). Connections were tested with custom hard- and software. Noise data were recorded in order to spot potential flaws, allowing for repair or replacement. As a final test, signals from cosmic muons originating from air-showers and traversing the detector were recorded and used for various studies, including alignment [7, 8].

Figure 4 shows the experimental setup. During cosmic muon data taking, TEC+ was in a vertical position (disk planes horizontal). Two square areas of size  $80\text{ cm} \times 80\text{ cm}$ , one below and one above the TEC+ sector under study, were covered with four AMS [13] scintillator panels [14], equipped with two photo-multipliers on opposite sides. A coincidence signal from one of the upper scintillator panels and one of the lower panels was demanded to trigger a readout of the TEC+ sector. A 10 cm thick lead shield was placed below TEC+, but above the lower scintillators, in order to absorb low energy ( $< 250\text{ MeV}$ ) muons and prevent them from triggering readout.

Customized CMS software was used to read out the detector, detect signals, and reconstruct tracks. Table 1 shows the number of triggers and reconstructed tracks used for alignment for each sector in chronological order.

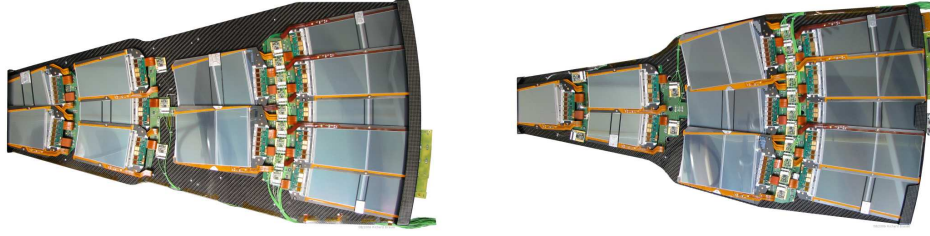


Figure 3: A TEC front petal (left) and a back petal (right) [7]. Only detector units on the side facing the interaction point can be seen (rings 1, 3, 5, and 7). Detector units on rings 2, 4, and 6 are located on the back side of the petal.

## 4.3 Results

### 4.3.1 Track selection

Tracks were reconstructed with bloated hit uncertainties in order to allow an efficient track reconstruction in the presence of misalignment and selected with loose criteria. To account for the overestimate, tracks with a  $\chi^2$ -probability  $P(\tilde{\chi}^2, n_{dof}) < 0.5$  with  $\tilde{\chi}^2$  from Eq. (10) were rejected.

After this selection, 4000 to 6000 tracks were available for each of the sectors 1, 3, 5 and 7. Due to an optimized trigger configuration, which took place only after integration of the odd-numbered sectors, there were between 35 000 and 60 000 tracks available for the even-numbered sectors 2, 4, 6 and 8. In total, the sector test data contain about 220 000 tracks which were used in alignment studies.

The starting geometry for the linearization of Eq. (3) was the design geometry, and the resulting measurements, predictions, derivatives, and covariance matrices were stored.

### 4.3.2 Disk alignment

Higher level structures like TEC petals and disks were aligned. Here, we describe the alignment of TEC disks, for which determined alignment parameters can be compared directly to measurements from survey and the Laser Alignment System (LAS).

Each of the eight TEC+ sectors has been tested separately. Therefore, no information can be gathered from the collected data about the relative position of the sectors with respect to each other. TEC+ disks were aligned by using all available tracks and assuming that detector elements were mounted on their nominal position on the petals, and petals on their nominal position on the disks. For each disk, corrections  $\Delta x$ ,  $\Delta y$ , and  $\Delta\phi$  were calculated. The corrections to the geometry have the same absolute value as the alignment parameters in Eq. (6), but with inverted sign.

The Kalman Filter alignment algorithm was configured to use zero as the initial value of the alignment parameters, corresponding to design geometry. The covariance matrix was initialised with large startup errors of 10 cm and 10 rad for spatial and angular parameters, respectively, to avoid biasing the alignment results by the starting values. The reference system was defined by assigning very small initial uncertainties of  $10^{-5}$  cm and  $10^{-5}$  rad to the  $x$ ,  $y$ , and  $\phi$  parameters, respectively, for the disk closest to the interaction region. A standard annealing configuration with  $b = 10\,000$  and  $n = 100$  was used. Tracks which resulted in an update of the parameters larger than the parameter uncertainty were rejected as outliers.

Table 1: Sector test data sets in chronological order.

Run number	Sector	Number of triggers	Number of tracks
20944 - 20952	5	87400	6961
21136 - 21163	3	122058	5821
21238 - 21269	1	88591	5807
21428 - 21448	7	83772	8502
21512 - 21530	2	82139	62650*
21592 - 21617	6	87258	68210*
21666 - 21670	4	58248	42260*
21713	8	73227	61159*

\*optimized trigger configuration

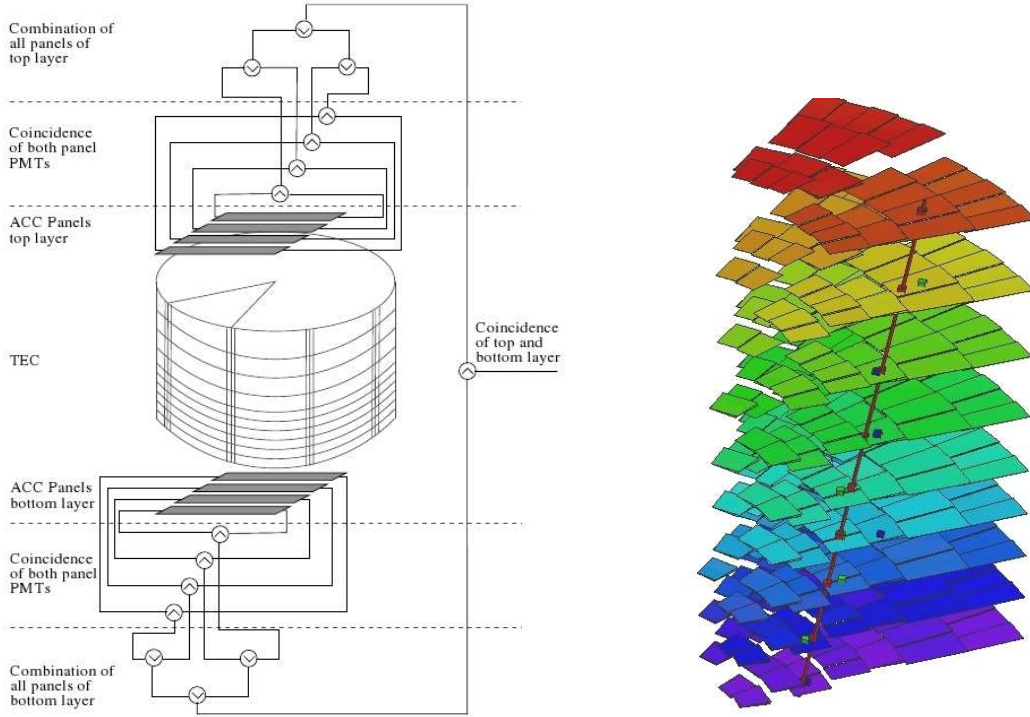


Figure 4: Cosmic trigger setup during TEC+ sector tests [7] (left). Reconstructed track of a muon traversing the nine disks of the TEC+ (right). Hits used by the track fitting algorithm are displayed in green, all remaining hits are coloured blue.

To verify convergence, several starting points for the parameters were tried and the order in which the data were processed was changed from chronological to random order. In both cases no significant changes in the resulting alignment parameters was observed.

Due to the low number of aligned parameters, the time used for computing the alignment constants, roughly 300 s, was dominated by input/output operation of the input data.

Due to the nature of the problem, the objective function only changes minimally when the linear transformations

$$\begin{aligned}\Delta x(z) &= \Delta x'(z) + a_x + b_x \cdot z \\ \Delta y(z) &= \Delta y'(z) + a_y + b_y \cdot z \\ \Delta \phi(z) &= \Delta \phi'(z) + a_\phi + b_\phi \cdot z\end{aligned}$$

are applied to the parameters, where  $z$  is the coordinate shown in Figure 1. These transformations correspond to weakly determined deformations of the TEC+ structure. The computed alignment parameters were, after the alignment procedure ended, transformed such that

$$\begin{aligned}\sum_i \Delta x_i \cdot z_i &= 0 \\ \sum_i \Delta x_i &= 0\end{aligned}$$

and corresponding constraints for the  $\Delta y_i$  and  $\Delta \phi_i$  were fulfilled.

Figure 5 shows the corrections  $\Delta x$  for disks 3 and 9 as a function of the number of processed tracks. It can be seen that the uncertainty on the correction decreases with the number of processed tracks. The uncertainty is larger for corrections belonging to alignables which are farther away from the disk that is used as the reference system (disk 1).

Table 2 lists the obtained alignment corrections together with their errors. The result is also displayed graphically in Figure 6. The size of the corrections is of order  $100 \mu\text{m}$  in  $x$  and  $y$ , and  $100 \mu\text{rad}$  in  $\phi$ , which corresponds

to an arc length of about  $100\ \mu\text{m}$  at the outer disk circumference. The accuracy of the positional and rotational corrections,  $2\text{--}10\ \mu\text{m}$  and  $2\text{--}10\ \mu\text{rad}$ , respectively, is very high compared to the typical size of the correction.

Table 2: Alignment corrections obtained from disk alignment in  $x, y, \phi$

Disk number	$\Delta x$ [ $\mu\text{m}$ ]	$\Delta y$ [ $\mu\text{m}$ ]	$\Delta\phi$ [ $\mu\text{rad}$ ]
1	$24 \pm 8$	$-99 \pm 8$	$33.6 \pm 7.3$
2	$60 \pm 6$	$-77 \pm 6$	$45.3 \pm 5.6$
3	$-20 \pm 4$	$17 \pm 4$	$51.2 \pm 4.1$
4	$-26 \pm 3$	$76 \pm 3$	$-53.6 \pm 2.7$
5	$83 \pm 2$	$146 \pm 2$	$-117.0 \pm 1.7$
6	$-162 \pm 2$	$42 \pm 2$	$-111.4 \pm 1.9$
7	$-67 \pm 4$	$21 \pm 4$	$115.8 \pm 3.7$
8	$7 \pm 6$	$-51 \pm 7$	$29.9 \pm 6.2$
9	$100 \pm 10$	$-74 \pm 10$	$6.2 \pm 9.2$

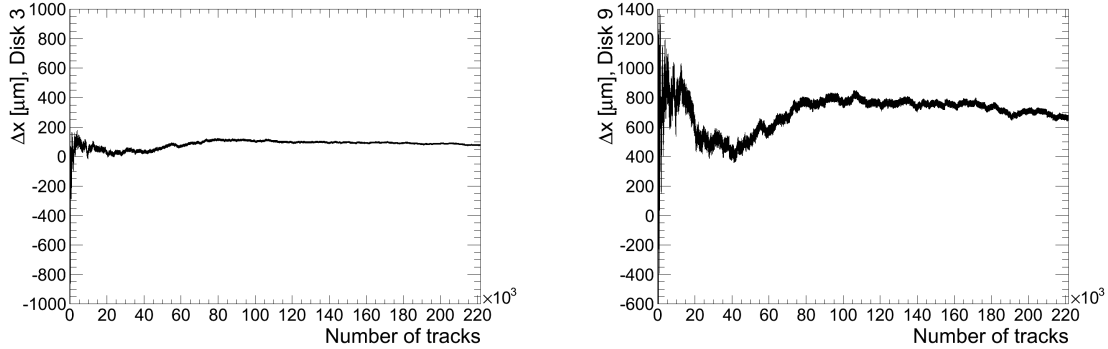


Figure 5: Corrections  $\Delta x$  for disks 3 (left) and 9 (right) as a function of the number of processed tracks. The width of the band represents the uncertainty on the correction.

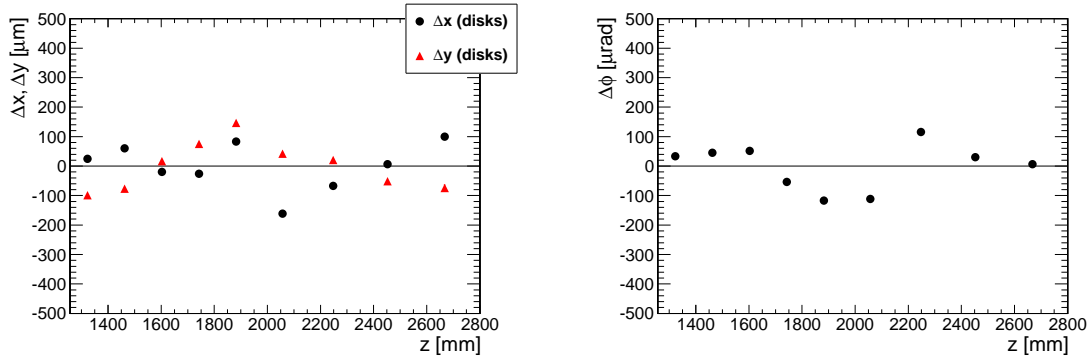


Figure 6: Alignment corrections for disk alignment in  $x, y, \phi$ . Error bars are smaller than the symbol size.

### 4.3.3 Comparison to Laser Alignment System results

The TEC also comprises a hardware alignment system [3], using sixteen laser rays of wavelength  $\lambda = 1075\ \text{nm}$  propagating parallel to the beam line. All rays pass through the back petals, eight rays pass at a radial distance  $r_4 = 564\ \text{mm}$  and eight further rays at  $r_6 = 840\ \text{mm}$ , the subscript indicating the ring number. The rays pass through an opening in the silicon detector's backside metallization. The laser rays get partially absorbed and produce signal on the detector elements. Using a straight line hypothesis, residuals can be deduced. These residuals were used to determine corrections to position and rotation of the nine TEC disks,  $\Delta x$ ,  $\Delta y$ , and  $\Delta\phi$  [15]. The corrections are listed in Table 3 and compared to the results deduced from the Kalman Filter in Figure 7.

The RMS of the differences between Laser Alignment System and Kalman Filter corrections is  $70\ \mu\text{m}$  in  $\Delta x$ ,  $52\ \mu\text{m}$  in  $\Delta y$ , and  $56\ \mu\text{rad}$  in  $\Delta\phi$ . Although overall good agreement is observed, some measurements deviate significantly. However, perfect agreement is not expected since the Laser Alignment System relies exclusively on 144 measurements of detector elements in rings 4 and 6 of back petals only, whereas the track based alignment



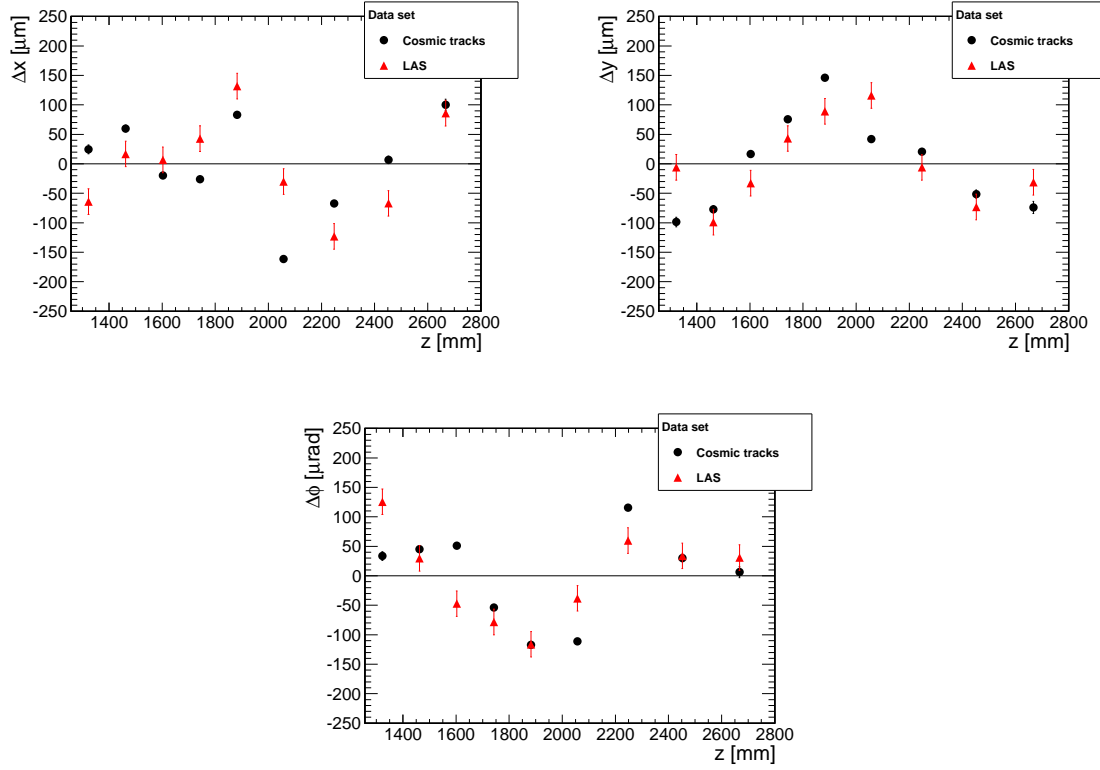


Figure 7: Comparison of Laser Alignment System [15] and track-based alignment results.

comprises data from more than 3000 modules on both front and back petals. In a further analysis it was found that the differences are compatible with the mounting precision of the petals. Especially the large deviation in  $\Delta x$  and  $\Delta y$  for the disk at  $z \approx 2050$  mm could be traced back to an imperfect front petal mounting in sector eight. Here, one of the precision pins with which the petals are attached to the disks was visually confirmed to be bent into the direction indicated by the alignment corrections.

Interpreting the result, the largest contribution to the misalignment is due to the positioning of the disks in the TEC+, and the remaining difference is to a large extent due to the positioning of the petals on the disks. This is in agreement with the naïve expectation that smaller structures can be assembled and mounted with higher precision than larger structures.

#### 4.3.4 Comparison to survey measurements

A further validation of the alignment results was performed with survey data recorded by a survey team before integrating the petals and after their integration. Using photogrammetry, the displacements of four points at the outer circumference of each disk were measured with a precision of about  $60 \mu\text{m}$ . Each measurement was done once with the TEC+ being in horizontal and once with it being in vertical orientation. As before, corrections  $\Delta x$  and  $\Delta y$  to the disk position as well as  $\Delta\phi$  to the disk rotation were estimated from these measurements.

Table 3: Displacements  $\Delta x$ ,  $\Delta y$ ,  $\Delta\phi$  of TEC+ disks determined with LAS residuals. The precision of the position corrections  $\Delta x$  and  $\Delta y$  is  $23 \mu\text{m}$ , and  $\Delta\phi$  is determined with an accuracy of  $23 \mu\text{rad}$ .

Disk number	$\Delta x$ [ $\mu\text{m}$ ]	$\Delta y$ [ $\mu\text{m}$ ]	$\Delta\phi$ [ $\mu\text{rad}$ ]
1	-64	-6	126
2	17	-99	30
3	7	-33	-47
4	43	43	-78
5	132	89	-116
6	-30	116	-38
7	-123	-6	60
8	-67	-73	34
9	86	-31	31

The measurements were transformed into the same reference system as used for the track-based alignment and are listed in Table 4. A graphical comparison of the track-based alignment results and survey data is given in Figure 8. The track-based alignment results agree with the survey measurements within (RMS)  $63 \mu\text{m}$  in  $\Delta x$ ,  $52 \mu\text{m}$  in  $\Delta y$ , and  $34 \mu\text{rad}$  in  $\Delta\phi$  and show, within measurement precision, good agreement.

Table 4: Displacements  $\Delta x$ ,  $\Delta y$ ,  $\Delta\phi$  of TEC+ disks determined with survey measurements. The precision of the position corrections  $\Delta x$  and  $\Delta y$  is  $57 \mu\text{m}$ , and  $\Delta\phi$  is determined with an accuracy of  $47 \mu\text{rad}$ .

Disk number	$\Delta x$ [ $\mu\text{m}$ ]	$\Delta y$ [ $\mu\text{m}$ ]	$\Delta\phi$ [ $\mu\text{rad}$ ]
1	30	-63	63
2	81	-54	19
3	-15	-15	57
4	18	6	-5
5	-31	110	-177
6	-73	158	-55
7	-165	-21	125
8	1	-64	20
9	154	-56	5

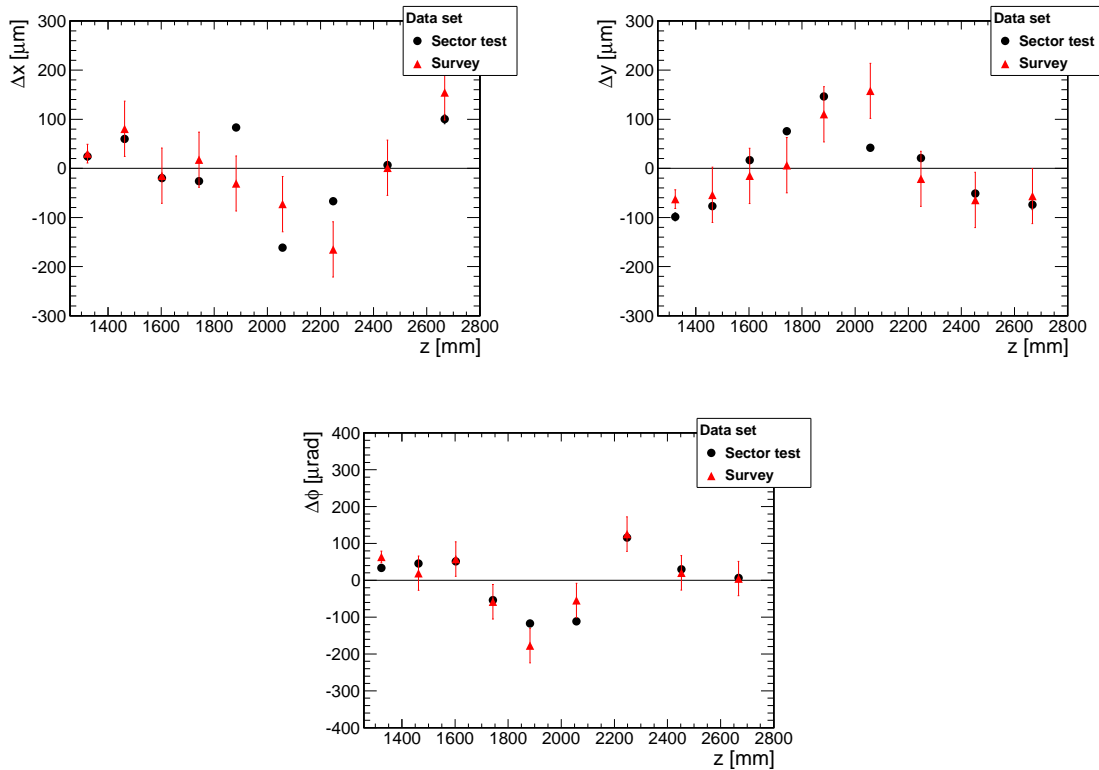


Figure 8: Comparison of survey and track-based alignment results.

## 5 Summary

A Kalman Filter alignment algorithm has been implemented in an experiment-independent way and applied to data. The obtained alignment corrections have been validated with both a hardware alignment system and survey data. The difference (RMS) between the corrections estimated with the track-based alignment and the hardware alignment system is  $70 \mu\text{m}$  and  $52 \mu\text{m}$  in  $\Delta x$  and  $\Delta y$ , respectively, and  $56 \mu\text{rad}$  in  $\Delta\phi$ . The track-based alignment results agree with the survey measurements within (RMS)  $63 \mu\text{m}$  in  $\Delta x$ ,  $52 \mu\text{m}$  in  $\Delta y$ , and  $34 \mu\text{rad}$  in  $\Delta\phi$ . The difference between laser alignment and survey data consistently is of a similar magnitude. Statistical uncertainties on the obtained alignment corrections are negligible when compared to the statistical uncertainties of laser alignment and survey data.

## Acknowledgements

We would like to thank Rudi Frühwirth, Wolfgang Adam and Edmund Widl for giving us insight into the Kalman Filter alignment algorithm.

## References

- [1] The BABAR Collaboration, B. Aubert *et al.*, Nucl. Inst. Methods **A479**, 1 (2002).
- [2] ATLAS Collaboration, “*The ATLAS Experiment at the CERN Large Hadron Collider*”, 2008 JINST 3 S08003, 2008.
- [3] CMS Collaboration, “*The CMS experiment at the CERN LHC*”, 2008 JINST 3 S08004 (2008).
- [4] V. Blobel and C. Kleinwort, “*A New Method for the High-Precision Alignment of Track Detectors*”, Proceedings Phystat2002, Durham (2002). (arXiv:hep-ex/0208021).
- [5] D. N. Brown, A. V. Gritsan, Z. J. Guo and D. Roberts, “*Local Alignment of the BABAR Silicon Vertex Tracking Detector*,” Nucl. Inst. Meth., in press, (doi:10.1016/j.nima.2009.02.001). (arXiv:0809.3823v1)
- [6] R. Frühwirth, T. Todorov and M. Winkler, “*Estimation of detector alignment parameters using the Kalman Filter with annealing*”, J.Phys. **G**: Nucl. Part. Phys. 29, 561–574 (2003).
- [7] V. Adler *et al.*, “*Integration of the End Cap TEC+ of the CMS Silicon Strip Tracker*”, CMS Note 2009/009 (2006).
- [8] Daniel Sprenger, “*Track-based Alignment of a CMS Tracker Endcap*”, CMS Thesis 2008/025 (2008).
- [9] E. Widl, R. Frühwirth, W. Adam, “*A Kalman Filter for Track-based Alignment*”, CMS Note 2006/022 (2006).
- [10] Rene Brun and Fons Rademakers, “*ROOT - An Object Oriented Data Analysis Framework*”, Proceedings AI-HENP’96 Workshop, Lausanne, Sep. 1996, Nucl. Inst. Meth. in Phys. Res. **A 389** (1997). (<http://root.cern.ch/>).
- [11] Bjarne Stroustrup, “*The C++ Programming Language (Special Edition ed.)*”, Addison-Wesley (2000). (ISBN 0-201-70073-5).
- [12] Lyndon Evans and Philip Bryant (editors), “*LHC Machine*”, 2008 JINST 3 S08001 (2008).
- [13] M. Aguilar *et al* (AMS-01 Collaboration) “*The Alpha Magnetic Spectrometer (AMS) on the International Space Station : Results from the test flight on the Space Shuttle*”, Phys. Rep. 366 (2002).
- [14] T. Bruch and W. Wallraff, “*The Anti-Coincidence Counter shield of the AMS tracker*”, Nucl. Inst. Meth. in Phys. Res. **A 572**, Issue 1, (2007).
- [15] Bruno Wittmer *et al.*, “*The Laser Alignment System for the CMS Silicon Microstrip Tracker*”, Nucl. Inst. Meth. in Phys. Res. **A 581** (2007). (doi:10.1016/j.nima.2007.08.002).